Synthesis, structure and electrochemical properties of K-based sulfates K 2 M2 (SO 4)3 with M = Fe and Cu

Laura Lander, Gwenaëlle Rousse, Dmitry Batuk, Claire Colin, Daniel Alves Dalla Corte, Jean-marie Tarascon

Synthesis, structure and electrochemical properties of K-based sulfates $K_2M_2(SO_4)_3$ with *M* = Fe and Cu

Laura Lander[a,b,c], Gwenaëlle Rousse[a,b,c,d], Dmitry Batuk[a,e], Claire V. Colin[f,g], Daniel Alves Dalla Corte[a] and Jean-Marie Tarascon[a,b,c*]

[a] UMR 8260 "Chimie du Solide et Energie", Collège de France, 11 Place Marcelin Berthelot, 75231 Paris Cedex 05, France.
[b] Réseau sur le Stockage Electrochimique de l'Energie (RS2E), FR CNRS 3459, France.
[c]Sorbonne Universités - UPMC Univ Paris 06, 4 Place Jussieu, F-75005 Paris, France.
[d] Institut Universitaire de France, 1 rue Descartes, 75231 Paris Cedex 05, France.
[e] EMAT, University of Antwerp, Groenenborgerlaan 171, B-2020 Antwerp, Belgium.
[f] Univ. Grenoble Alpes, Institut Néel CNRS, 38042 Grenoble, France.
[g] CNRS, Institut Néel, F-38000 Grenoble, France.

* Corresponding author: jean-marie.tarascon@college-de-france.fr

Abstract

Stabilizing new host structures through potassium extraction from K-based polyanionic materials has been proven to be an interesting approach to develop new Li^+/Na^+ insertion materials. Pursuing the same trend, we here report the feasibility of preparing langbeinite "$Fe_2(SO_4)_3$" via electrochemical and chemical oxidation of $K_2Fe_2(SO_4)_3$. Additionally, we succeeded in stabilizing a new $K_2Cu_2(SO_4)_3$ phase via solid-state synthesis approach. This novel compound crystallizes in a complex orthorhombic structure that differs from that of langbeinite as deduced from synchrotron X-ray and neutron powder diffraction. Electrochemically-wise the performance of this new phase is limited, which we explain in terms of sluggish diffusion kinetics. We further show that $K_2Cu_2(SO_4)_3$ transforms into $K_2Cu_3O(SO_4)_3$ on heating and we report for the first time the synthesis of fedotovite $K_2Cu_3O(SO_4)_3$. Lastly, the fundamental attractiveness of these S=1/2 systems for physicists is examined by neutron magnetic diffraction, which reveals the absence of a long-range ordering of Cu^{2+} magnetic moments down to 1.5 K.

Keywords

Langbeinite $K_2Fe_2(SO_4)_3$, sulfates, Cu-based polyanionic compounds, diffusion properties, $K_2Cu_2(SO_4)_3$, fedotovite $K_2Cu_3O(SO_4)_3$, solid-state synthesis

Introduction

Over the last few years, sustainability has become an overriding factor in the search for new electrode materials. The discovery of the electrochemical activity of $LiFePO_4$ *vs.* $Li^+/Li°$ back in 1997 was an impetus to further explore polyanionic materials for battery applications.[1,2] In this context, the finding of tavorite and triplite $LiFeSO_4F$ with potentials of 3.6 V and 3.9 V *vs.* Li^+/Li^0 was an important step forward.[3–5] Owing to the attractive electrochemical performances of the $LiFeSO_4F$ polymorphs further research efforts were undertaken to stabilize novel "$FeSO_4F$" frameworks for Li^+ and Na^+ insertion. This led to the discovery of orthorhombic and monoclinic $KFeSO_4F$, which form new polymorphic "$FeSO_4F$" host structures upon K^+ extraction.[6–8] Among them, the orthorhombic "$FeSO_4F$" phase displayed appealing cycling behavior towards Li and Na. This approach was further extended to phosphate-based phases such as $KVPO_4F$.[9]

Bearing this in mind, we embarked on the search of new sulfate-based host structures, which could uptake alkali cations. We focused our attention on various $A_2Fe_2(SO_4)_3$ phases with *A*=Li, Na, K that present polymorphic "$Fe_2(SO_4)_3$" frameworks. $Li_2Fe_2(SO_4)_3$ crystallizes in the Nasicon and anti-Nasicon structures, both displaying a potential of 3.6 V *vs*. Li^+/Li^0, while $Na_2Fe_2(SO_4)_3$ presents the alluaudite-type structure with a potential of 3.8 V *vs.* Na^+/Na^0.[10–13] Another "$Fe_2(SO_4)_3$" framework is based on the family of the langbeinite phases having the general composition $A_2M_2(SO_4)_3$, with *A* = K, NH_4, Rb, Tl and *M* = Mg, Mn, Ni, Zn, Ca, Fe, Cd and Co. The langbeinite compounds are derived from the mineral $K_2Mg_2(SO_4)_3$ and have been vastly studied for their physical properties including antiferromagnetic spin-ordering, electro-optical effects as well as ferroelectric and ferroelastic features.[14–21] However, to the best of our knowledge, their electrochemical properties have not been reported so far. Hence our goal was to explore the feasibility of preparing a stable langbeinite "$Fe_2(SO_4)_3$" framework upon K^+ extraction from $K_2Fe_2(SO_4)_3$. Moreover, through the investigation of other langbeinite $A_2M_2(SO_4)_3$ phases, we have isolated a new $K_2Cu_2(SO_4)_3$ member that presents a noticeably different crystal structure as compared to cubic $K_2Fe_2(SO_4)_3$. This phase shows limited electrochemical activity and transport properties. It is thermally unstable and decomposes to form the fedotovite oxysulfate $K_2Cu_3O(SO_4)_3$ above 320°C. Lastly, we examined the possibility

of long range magnetic ordering of Cu^{2+} in $K_2Cu_2(SO_4)_3$ and $K_2Cu_3O(SO_4)_3$ via low-temperature neutron diffraction experiments.

Experimental part

Laboratory X-ray diffraction (XRD) patterns were recorded with a Bruker D8 Advance diffractometer equipped with a copper source ($\lambda_{Cu\text{-}K\alpha1}$ = 1.54056 Å, $\lambda_{Cu\text{-}K\alpha2}$ = 1.54439 Å) and a LynxEye detector. For high temperature XRD experiments, the diffractometer was equipped with an Anton Paar HTK1200N furnace. Synchrotron X-ray diffraction patterns were measured in transmission mode (the powder was placed in a Ø=0.7 mm capillary sealed under argon), with a wavelength of λ=0.4141 Å at the 11BM beam line at Argonne National Lab. Neutron powder diffraction (NPD) experiments were performed on the D1B powder diffractometer at the Institut Laue Langevin, with a wavelength of 2.529 Å and with the powder placed in a Ø=6mm vanadium can. The recorded patterns were refined using the Rietveld[22] method as implemented in the FullProf[23,24] program. Bragg peak indexation and structure determination were performed with help of the Dicvol[25,26] and Fox[27,28] programs.

For transmission electron microscopy measurements, a FEI Tecnai G2 electron microscope operated at 200 kV was used. For the measurement, the sample was prepared in an Ar-filled glove box by grinding the powder in a mortar in anhydrous hexane and depositing drops of suspension onto holey carbon grids. The sample was transported to the microscope column completely excluding contact with air.

Electrochemical tests were conducted in Swagelok-type cells assembled in an argon-filled glovebox and cycled in a galvanostatic operating mode using a VMP system (Biologic S.A., Claix, France). Lithium metal was used as the negative electrode and the working electrode consisted of a composite of the active material and Carbon SP (Csp) (80:20 wt %), prepared by ball-milling for 15 min in a Spex 8000 miller. The negative and the positive electrode were separated by a Whatman GF/D borosilicate glass fiber sheet saturated with 1 M $LiPF_6$ in EC:DMC (1:1 weight ratio) (LP30).

A.c. impedance measurements were performed with a Bio-Logic MTZ-35 Impedance Analyzer, in a frequency range of 1 MHz to 0.1 Hz and with an excitation voltage of 100 mV. The

measurements were done under argon at various stabilized temperatures ranging from 100 to 450°C.

Results

a) Synthesis and Electrochemistry of $K_2Fe_2(SO_4)_3$

In previous reports, langbeinite $K_2Fe_2(SO_4)_3$ was prepared from an aqueous solution of K_2SO_4 and $FeSO_4$.[19,29] Herein, we simply prepared this phase by ball-milling stoichiometric amounts of K_2SO_4 and anhydrous $FeSO_4$ with a Spex 8000 vibratory miller for 1 h. The powders were placed in a hermetic stainless-steel jar filled in an argon dry box. A ball-to-powder weight ratio of ~30 was used. Afterwards, the composite mixture was annealed at 400 °C for 7 h under argon atmosphere to produce a single phase powder as deduced by X-ray diffraction (XRD). The Rietveld refinement[22–24] of as-prepared $K_2Fe_2(SO_4)_3$ was performed with an initial structural model constructed from $K_2Mn_2(SO_4)_3$,[15] where Mn was replaced by Fe, and all atoms were freely refined. The final refinement is shown in Figure 1a and indicates that $K_2Fe_2(SO_4)_3$ and $K_2Mn_2(SO_4)_3$ are isotructural. $K_2Fe_2(SO_4)_3$ crystallizes in a cubic unit cell with lattice parameter a = 10.00476(4) Å. The structure, described in space group $P2_13$, consists of isolated FeO_6 octahedra (blue) that are connected to six SO_4 tetrahedra (light blue) via their oxygen (grey) vertices (Figure 1b). The K1 and K2 atoms, which are eight- and six-fold coordinated, respectively, are located in the large cavities of the $Fe_2(SO_4)_3$ framework. The structural data, including a bond valence sum analysis,[30] is summarized in Table 1.

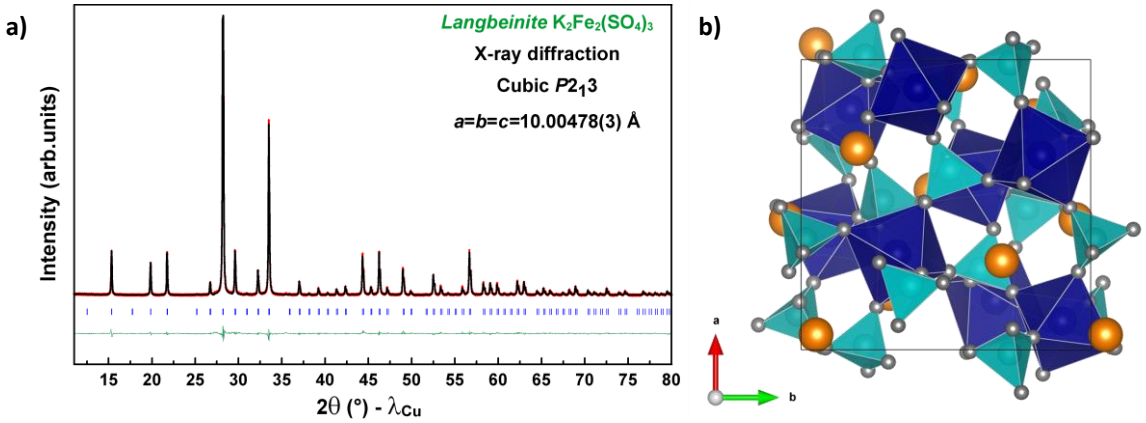

Figure 1: Rietveld refinement of the X-ray diffraction pattern of $K_2Fe_2(SO_4)_3$. The red crosses, black line, and green line represent the observed, calculated and difference patterns, respectively. The positions of the Bragg reflections are shown as vertical blue bars. b) Structure of $K_2Fe_2(SO_4)_3$, where the FeO_6 octahedra and SO_4 tetrahedra are shown in blue and light blue, respectively. O and K atoms are illustrated as grey and orange spheres.

Electrochemical tests were conducted in Swagelok-type cells with a lithium anode and a cycling regime of C/20 (1C equals the uptake or removal of 1 Li^+ in 1 h). A typical composition-voltage trace is shown in Figure 2a. On charge, we observe a pseudo-plateau at around 3.9 V vs. Li^+/Li^0 and a flat plateau at ~4.1 V vs. Li^+/Li^0, each accounting for approximately 0.2 K^+. On discharge, however, only ~0.2 Li^+ can be reinserted resulting in merely 10 % of the theoretical capacity (129 mAh/g) of $K_2Fe_2(SO_4)_3$. Further optimization trials of the cathode material (*e.g.* longer ball-milling, higher Csp content) did not improve the electrochemical performance.

To further check the extend of potassium removal, we conducted chemical oxidation of $K_2Fe_2(SO_4)_3$ using NO_2BF_4 as oxidizing agent in acetonitrile under reflux (~ 80°C) for times ranging from 5 hours to 2 days. XRD of the resulting $K_{2-x}Fe_2(SO_4)_3$ compound indicates a minor shift of the Bragg peaks (Figure 2b, blue pattern), as well as a tiny amount of KBF_4 (peak marked with asterisk), resulting from the reaction of NO_2BF_4 with the extracted K^+. However, its amount did not increase with increasing reaction time, thus confirming the difficulties of K^+ extraction encountered during the electrochemical cycling. Lastly, the neat superimposition of the XRD patterns of the K-deficient samples (Figure 2b) prepared by chemical and electrochemical oxidation indicates that the same amount of K^+ is extracted for both routes and it is limited to values lower than ~0.4 K^+ per formula unit (see voltage-composition trace, Figure 2a). In addition to the poor reversibility observed during the electrochemical discharge, the existence of large voltage polarization suggests sluggish diffusion kinetics. This does not come as a surprise given the high percolation energy of 7.8 eV as calculated by the Bond

Valence Energy Landscape (BVEL) approach (described in detail in SI; Figure SI1a).[23,31] This value exceeds by far the BVEL percolation energies of other sulfate-based materials (~0.5 - 3 eV)[8,32,33], hence indicating a hampered K^+ diffusion. Problems during K^+ extraction were previously assessed for langbeinite $K_2TiV(PO_4)_3$, where chemical oxidation failed to remove K^+.[34] Moreover, it was reported that Li^+ and Na^+ are too small to generate a stable langbeinite framework.[29] This statement is also confirmed by our unsuccessful trials to prepare langbeinite $A_2Fe_2(SO_4)_3$ with A=Li or Na using a variety of precursors and methods as well as ionic substitution of $K_2Fe_2(SO_4)_3$ with $LiNO_3$ and $NaNO_3$. In short, these results show that $K_2Fe_2(SO_4)_3$ is not a suitable electrode material.

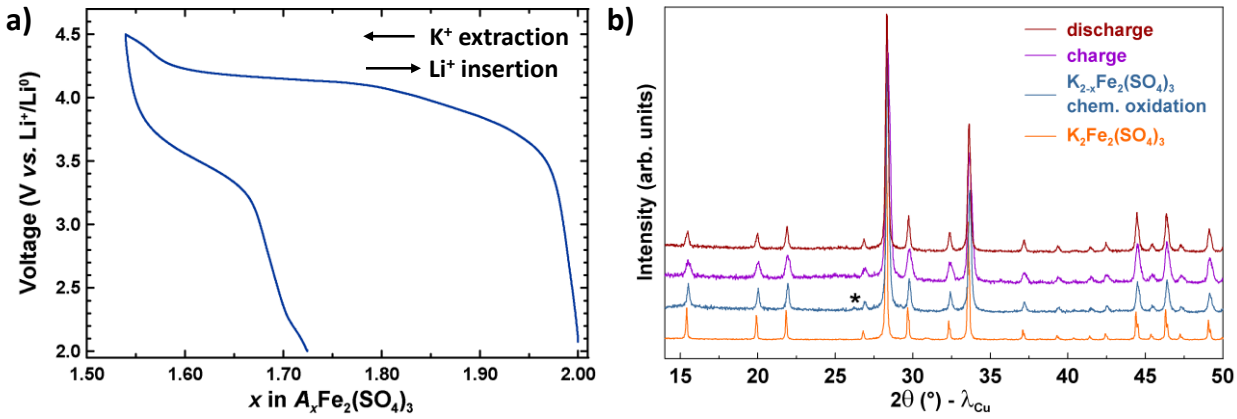

Figure 2: a) Voltage-composition trace of cubic $K_2Fe_2(SO_4)_3$. *A* in $A_2Fe_2(SO_4)_3$ corresponds to K^+ in the first charge and to Li^+ onwards. b) XRD pattern of pristine $K_2Fe_2(SO_4)_3$ (orange), chemically oxidized $K_{2-x}Fe_2(SO_4)_3$ (blue), electrochemically charged $K_{2-x}Fe_2(SO_4)_3$ (purple) and discharged $(K,Li)_2Fe_2(SO_4)_3$ (maroon). The asterisk marks the peak attributed to KBF_4.

b) Synthesis, structure and electrochemistry of $K_2Cu_2(SO_4)_3$

Aside from Fe-based sulfate compounds, we recently demonstrated the feasibility to achieve high redox potentials (> 4.6 V *vs.* Li^+/Li^0) in Cu-based sulfates/oxysulfates such as $Li_2Cu_2O(SO_4)_2$.[31] Interestingly, Gattow *et al.*[29] predicted that the Cu-based homologue of $K_2Fe_2(SO_4)_3$ might present a different crystal structure due to the preferential square-planar coordination of the Jahn-Teller active Cu^{2+}. All together this prompted us to explore the possibility of stabilizing $K_2Cu_2(SO_4)_3$ and study its properties.

Phase-pure $K_2Cu_2(SO_4)_3$ was successfully prepared by a two-steps solid-state route. First, stoichiometric amounts of K_2SO_4 and anhydrous $CuSO_4$ (Alfa Aesar, Reagent Grade), which has been dried under vacuum at 260 °C for 24 h, were ball milled for 4 h in an Ar-filled ball-mill jar

with a Spex 8000 vibratory miller with a ball-to-powder weight ratio of 25. The obtained mixture was then pressed to a pellet and heated at 300 °C for 20 h under constant argon flow. The resulting powder consists of particles in the sub-micrometer range (Figure SI2). It is worth mentioning at this point that like most of the alkali-based 3d metal sulfates, $K_2Cu_2(SO_4)_3$ is highly moisture sensitive and decomposes into $K_2Cu(SO_4)_2{\cdot}6H_2O$ and $CuSO_4{\cdot}5H_2O$ after solely 8 h of air exposure (Figure SI3). It is therefore important to synthesize and handle $K_2Cu_2(SO_4)_3$ under air- and moisture-free conditions.

In the absence of single crystals, the crystal structure of $K_2Cu_2(SO_4)_3$ was solved by combined synchrotron X-ray and neutron powder diffraction. With help of the Dicvol[25,26] program, the Bragg peaks in the synchrotron XRD patterns could be indexed in an orthorhombic unit cell with the lattice parameters a = 4.81065(1) Å, b = 11.91795(3) Å and c = 18.67516(4) Å and a volume of V = 1070.704(4) Å^3. This cell can accommodate four formulae units (Z = 4). We obtained in total 17 possible space groups that could index the observed reflections. Since no structural model was known for this compound, we performed *ab initio* structural determination methods for all possible space groups using the Fox[27,28] program and compared the obtained structural models to the experimental SXRD data. During this process, the SO_4 tetrahedra were treated as rigid groups. Besides the many possible space groups, the large number of atoms further complicated the search for the correct structural model. The only space group, which indexed all the Bragg peaks obtained by SXRD and resulted in a meaningful structure, was $P2_12_12_1$. Furthermore, this symmetry is corroborated by the electron diffraction data (collected on an FEI Tecnai G2 microscope). The observed reflection conditions $h00$: h = 2n; $0k0$: k = 2n; $00l$: l = 2n are consistent only with the space group $P2_12_12_1$ (Figure 3a). The final refinement of $K_2Cu_2(SO_4)_3$ with all atoms freely refined using the Rietveld method as implemented in the FullProf[23,24] program is shown in Figure 3b. The structural data deduced from this refinement are summarized in Table 2. Moreover, for a more accurate refinement of the O positions, we performed neutron powder diffraction on the D1B powder diffractometer, with a wavelength of 2.529 Å. The Rietveld refinement conducted on the NPD pattern is shown in Figure 3b and fully validates the structural model.

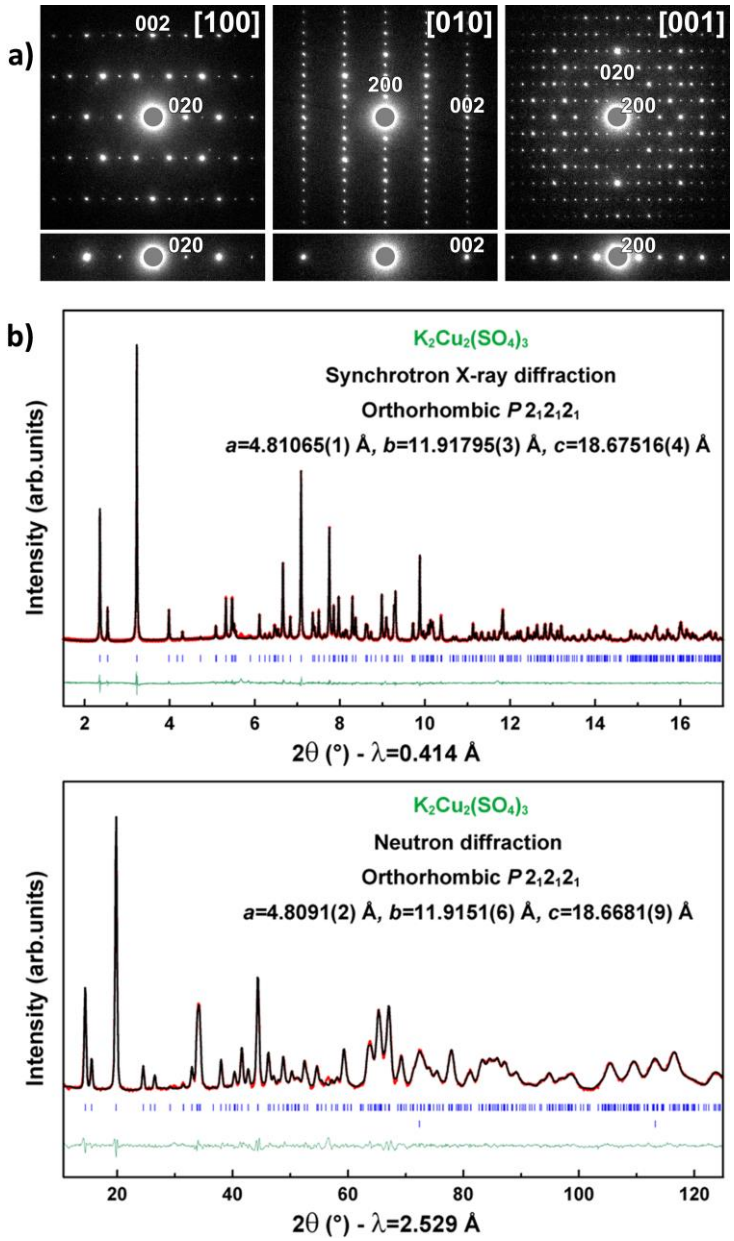

Figure 3: a) Electron diffraction data for $K_2Cu_2(SO_4)_3$. In the patterns taken along the main zone axis (square patterns), reflections violating *h*00: *h*=2n; 0*k*0: *k*=2n; 00*l*: *l*=2n extinction conditions reappear owing to the dynamical effects. The reflection conditions are unambiguously observed when the crystal is tilted away from the zone axis, so that only a single row of reflections fulfills the diffraction conditions (rectangular patterns). b) Rietveld refinement of the synchrotron XRD and neutron powder diffraction patterns of $K_2Cu_2(SO_4)_3$. The red crosses, black line, and green line represent the observed, calculated and difference patterns, respectively. The positions of the Bragg reflections are shown as vertical blue bars. The second phase in the neutron diffraction pattern stems from the vanadium can.

The 19 independent atoms of $K_2Cu_2(SO_4)_3$ are all located in the 4*a* general position of the $P2_12_12_1$ space group (Table 2). The structure of $K_2Cu_2(SO_4)_3$ is based on distinct infinite "$Cu_2(SO_4)_3$" chains running along [100] and forming a herringbone pattern in the *bc* plane (Figure 4a). Each of these chains consists of square-planar CuO_4 and square-pyramidal CuO_5 groups (Figure 4: CuO_4 and CuO_5 are connected through one oxygen vertices to form Cu_2O_8

entities, which are further bridged via SO_4 tetrahedra. The K1 and K2 atoms, which are eight-fold coordinated (Figure 4c), are located in the empty space between the chains. The oxidation states of the atoms calculated by bond valence sum analysis (Table 2) are consistent with what is expected for this composition.

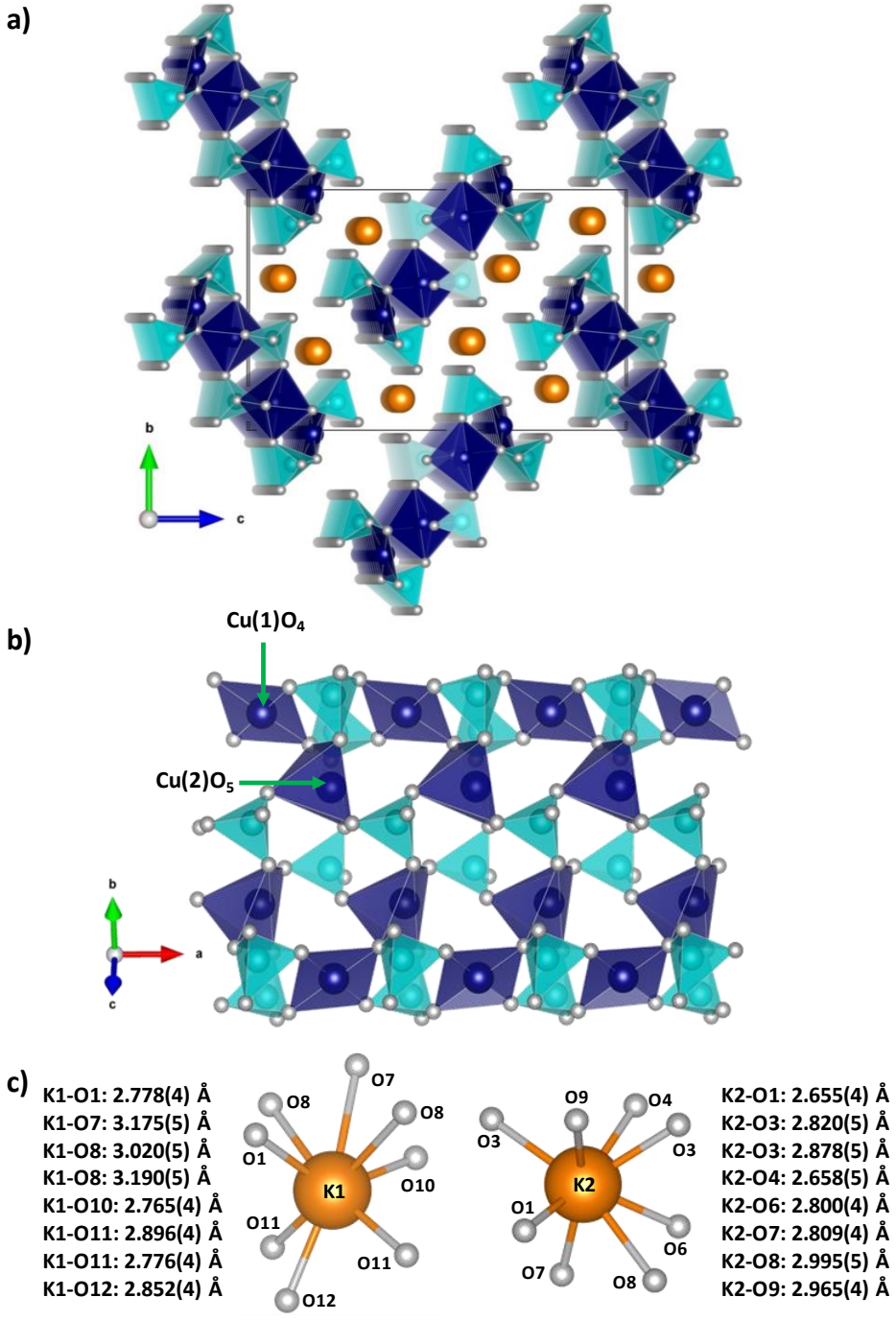

Figure 4: a) Structure of orthorhombic $K_2Cu_2(SO_4)_3$ shown along the [100] axis. The CuO_x polyhedra and SO_4 tetrahedra are shown in blue and red, respectively, with the oxygen atoms in grey. The potassium atoms are represented as yellow balls. b) Connectivity of the CuO_x polyhedra and SO_4 tetrahedra in $K_2Cu_2(SO_4)_3$. c) Local coordination of K1 and K2 with the respective K-O bond lengths.

Figure 5 shows the room temperature electrochemical behavior of a Li/$K_2Cu_2(SO_4)_3$ Swagelok-type cell using $K_2Cu_2(SO_4)_3$ ball milled for 15 min with Csp (weight ratio 80:20) as positive electrode, LP30 as electrolyte and cycled at a C/50 rate. The cell voltage profile (Figure 5a) presents a limited electrochemical activity (x ~ 0.1) being far from reaching the theoretical capacity of 124 mAh/g. The redox process proceeds via one plateau at 3.4 V *vs.* Li^+/Li^0 and two minor sloping contributions at 3.75 V *vs.* Li^+/Li^0 on charge and between 2.5-2.8 V *vs.* Li^+/Li^0 on discharge that can be also seen on the dx/dV derivative curve (Figure 5b). We observed that charging the Li/$K_2Cu_2(SO_4)_3$ to higher potentials such as 5 V *vs.* Li^+/Li^0 leads to a decomposition of the active material as deduced from traces of elemental copper on the separator of disassembled cells.

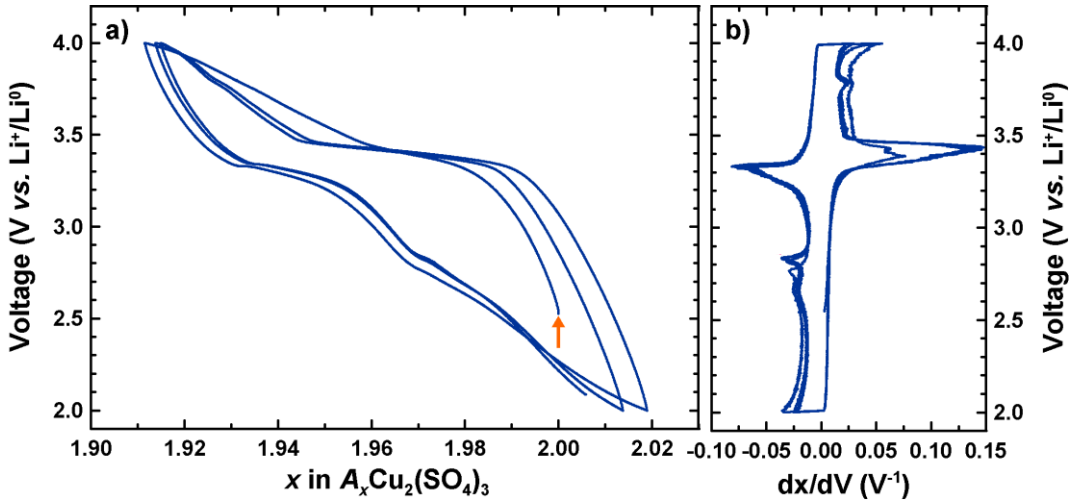

Figure 5: Voltage-composition trace of $K_2Cu_2(SO_4)_3$ cycled at C/50 started in oxidation (orange arrow) (a) and its derivative curve (b).

We further attempted to chemically remove K^+ from $K_2Cu_2(SO_4)_3$ by oxidation using an excess of NO_2BF_4 in acetonitrile. Figure 6 compares the XRD patterns of samples recovered from electrochemical cells, which were stopped on charge (purple pattern) and discharge (maroon pattern), respectively, with the pattern of the chemically oxidized (blue pattern) and the pristine (orange pattern) samples. They all look alike with no noticeable shift of the Bragg peaks. However, we observe the formation of KBF_4 (peaks marked with asterisk) for the chemically oxidized sample. From a Rietveld refinement (shown in Figure SI4), we could estimate the amount of KBF_4 to be 10(4) %, hence implying that ~10 % of K^+ was extracted, in good agreement with the electrochemical data.

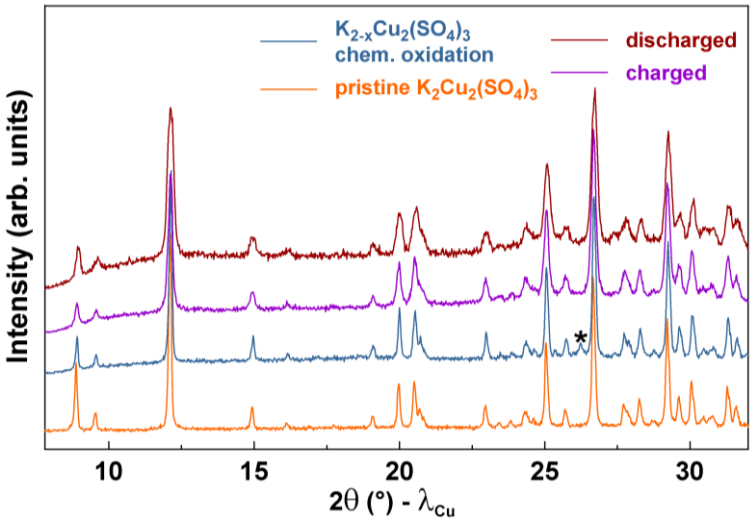

Figure 6: XRD patterns of pristine $K_2Cu_2(SO_4)_3$ (orange) and chemically oxidized $K_2Cu_2(SO_4)_3$ using NO_2BF_4 (blue pattern). The purple and red XRD patterns were recorded *ex situ* after charge and discharge of $K_2Cu_2(SO_4)_3$. The peak marked with * corresponds to KBF_4.

To rationalize the poor removal of K^+, we calculated the K^+ diffusion pathways via the Bond Valence Energy Landscape (BVEL) approach (Figure SI1b) and deduced an anisotropic diffusion of K^+ in this material with percolation energies of 1.59, 2.78 and 6.38 eV along the [100], [010] and [001] directions, respectively. To provide a real meaning to these values, temperature-dependent a.c. conductivity was measured on a sintered $K_2Cu_2(SO_4)_3$ pellet (Ø 10 mm, compactness 82%) between ionically blocking gold electrodes (Figure 7a). The measurements were done under argon at various stabilized temperatures ranging from 100 to 450°C in a frequency range of 1 MHz to 0.1 Hz and with an excitation voltage of 100 mV. A typical collected impedance spectrum (see inset Figure 7a) consists of a low frequency tail indicating that the conductivity is mainly ionic with in addition the presence of two semi-circles corresponding to the bulk contribution (high frequency) and the grain boundary (medium frequency). $K_2Cu_2(SO_4)_3$ presents an activation energy of 1.49 eV as deduced by fitting the a.c. data with the Arrhenius law and an extrapolated room temperature a.c. conductivity of $\sigma_{RT} = 10^{-13}$ S/cm. Compared to other polyanionic cathode materials such as $LiFePO_4$ and triplite $LiFeSO_4F$, which show activation energies of 0.6 eV and 0.79 eV, respectively,[35,36] $K_2Cu_2(SO_4)_3$ presents rather mediocre conductivity in agreement with the observed electrochemical performances. Note the sudden drop of conductivity of $K_2Cu_2(SO_4)_3$ upon heating at around 380 °C suggesting a possible phase transition (Figure 7b).

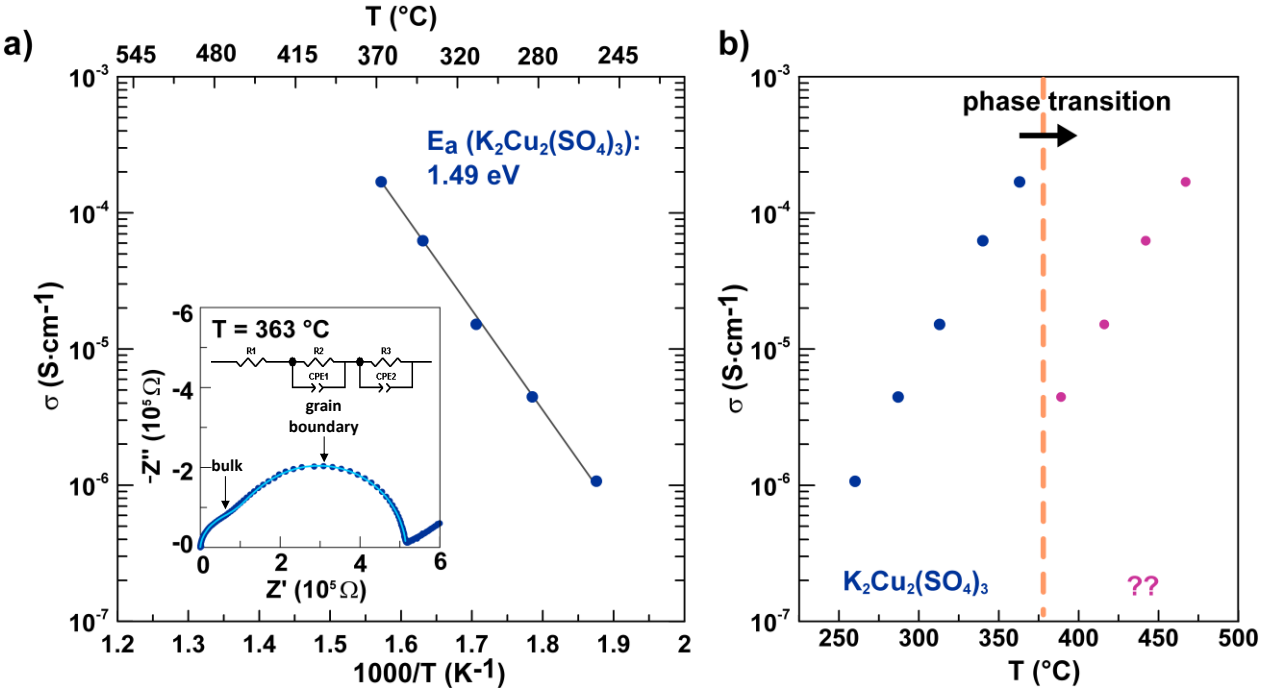

Figure 7: Temperature dependence of the a.c. conductivity of $K_2Cu_2(SO_4)_3$ and its activation energy E_a deduced from the Arrhenius equation (a). These activation energies are physically not related to the percolation energies deduced from BVEL. The inset shows the measured impedance spectrum at 363 °C and the circuit used for the fit. The observed drop of conductivity around 380 °C suggests a phase transformation (b).

To get more insight into this possible phase transformation, we performed high-temperature *in situ* XRD measurements (Figure 8), where $K_2Cu_2(SO_4)_3$ was heated under a steady nitrogen flow from 50 °C to 620 °C in 20 °C steps and with a ramp of 5 °C/min and cooled down to 100 °C again. The temperature was held constant at each step during the recording of the XRD pattern (1h). Pristine $K_2Cu_2(SO_4)_3$ is stable until 400 °C and presents only a thermal expansion of the structure. From 420 °C onwards a new peak appears at ~12°, which can be assigned to the mineral fedotovite $K_2Cu_3O(SO_4)_3$. The phase transformation from $K_2Cu_2(SO_4)_3$ to $K_2Cu_3O(SO_4)_3$ is completed at 500 °C, before the irreversible decomposition of $K_2Cu_3O(SO_4)_3$ at 560 °C. The slightly different transition temperatures seen from impedance measurements and in situ XRD are due to differences in heating ramps and heating dwells. The phase transformation, also confirmed by DSC measurements, can be directly visualized through a colour change from light blue for $K_2Cu_2(SO_4)_3$ to dark green for $K_2Cu_3O(SO_4)_3$ (Figure SI5).

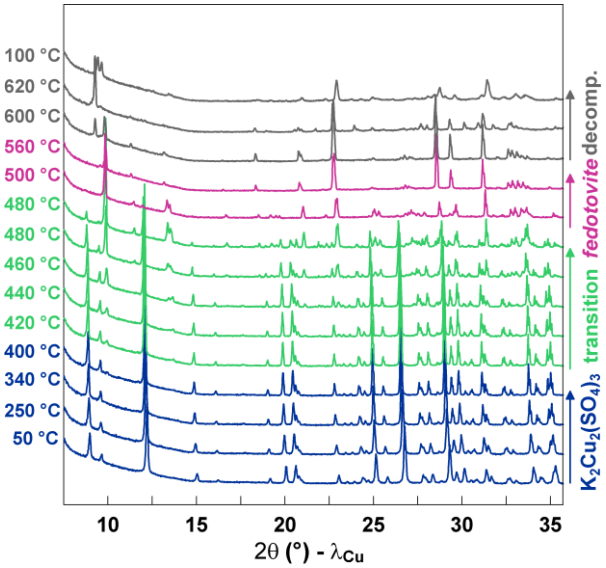

Figure 8: High-temperature *in situ* XRD experiment on $K_2Cu_2(SO_4)_3$, which was heated from 50 °C to 620 °C and cooled down to 100 °C under nitrogen flow. The blue, green and purple pattern correspond to the pristine $K_2Cu_2(SO_4)_3$, the transition range (biphasic domain) and to fedotovite $K_2Cu_3O(SO_4)_3$ respectively. The grey patterns correspond to decomposition products.

c) Synthesis and Structure of $K_2Cu_3O(SO_4)_3$

Fedotovite $K_2Cu_3O(SO_4)_3$ is a volcanic mineral, which was first discovered in Kamchatka, Russia, after a volcano eruption in 1975/1976.[37] It has only been characterized as a natural mineral, but, to the best of our knowledge, has never been obtained synthetically. We thus report here for the first time its synthesis protocol. For the preparation of $K_2Cu_3O(SO_4)_3$, we started either from $K_2Cu_2(SO_4)_3$, which was ball milled for 30 min with an excess of CuO (10 %) (Equation 1), or from the precursors K_2SO_4, $CuSO_4$ and CuO (Equation 2), which were ball-milled for 45 min. The mixtures were heated at 500 °C for 30-48 h under argon atmosphere.

$$K_2Cu_2(SO_4)_3 + CuO \rightarrow K_2Cu_3O(SO_4)_3 \quad \textbf{(1)}$$

$$K_2SO_4 + CuSO_4 + CuO \rightarrow K_2Cu_3O(SO_4)_3 \quad \textbf{(2)}$$

XRD experiments confirmed the purity of the sample. Rietveld refinements of the SXRD and neutron patterns of synthetically prepared $K_2Cu_3O(SO_4)_3$ were performed using the monoclinic *C*2/*c* structural model previously reported by Starova *et al.*[37] (Figure 9). The obtained structural data is given in Table 3. The slight differences of the lattice parameters of our prepared fedotovite phase (a = 19.09059(5) Å, b = 9.52853(2) Å, c = 14.18650(3) Å, β = 110.63109(19)° and V = 2415.100(9) Å^3) as compared to the one reported by Starova *et al.* (a = 19.037(6) Å, b = 9.479(2) Å, c = 14.231(5) Å, β = 111.04(3)°, corresponding to a unit cell

volume of V = 2396.8(3) Å^3)[37] might be related to the fact that their structure was solved on the mineral, which might contain impurities that influence the lattice size.

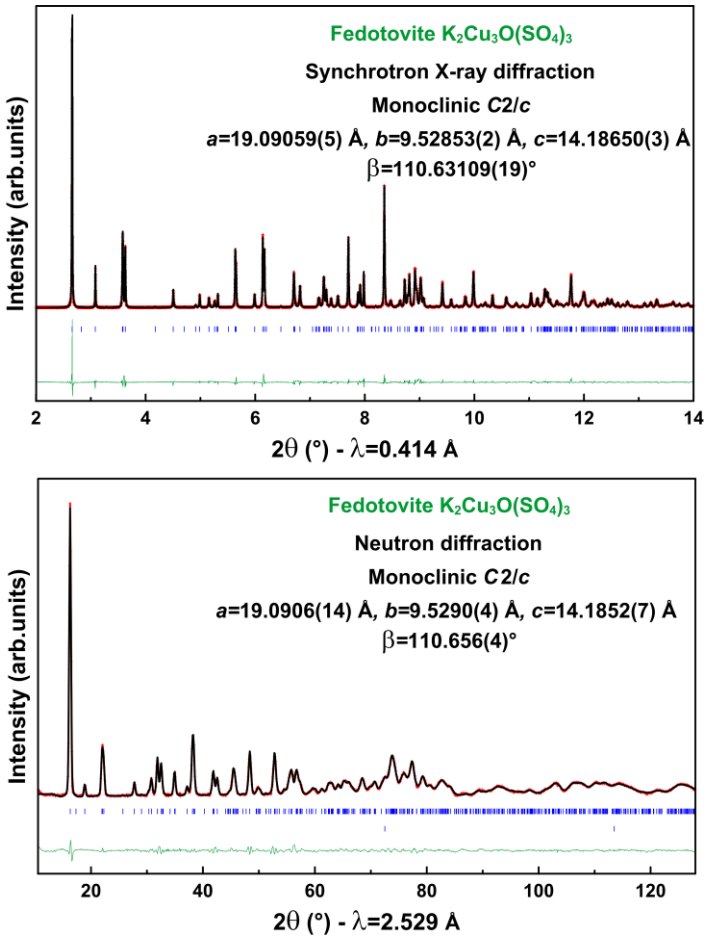

Figure 9: Rietveld refinement of the synchrotron X-ray powder diffraction (top) and neutron powder diffraction (bottom) of fedotovite $K_2Cu_3O(SO_4)_3$. Red, black and green lines represent the experimental, calculated and difference patterns, respectively. Bragg positions are shown as blue bars. The second phase in the neutron diffraction pattern stems from the vanadium can.

$K_2Cu_3O(SO_4)_3$ adopts a layered-like structure (Figure 10a). The layers are constructed on $Cu(1)O_5$ and $Cu(2)O_5$ square-based pyramids linked to $Cu(3)O_4$ planar entities via vertices, forming building blocks (Figure 10b, left) which are connected through SO_4 tetrahedral groups. Potassium atoms are located between the layers. Note that the two coordination modes of copper in this $K_2Cu_3O(SO_4)_3$ structure are also present in $K_2Cu_2(SO_4)_3$ (Figure 10b, right).

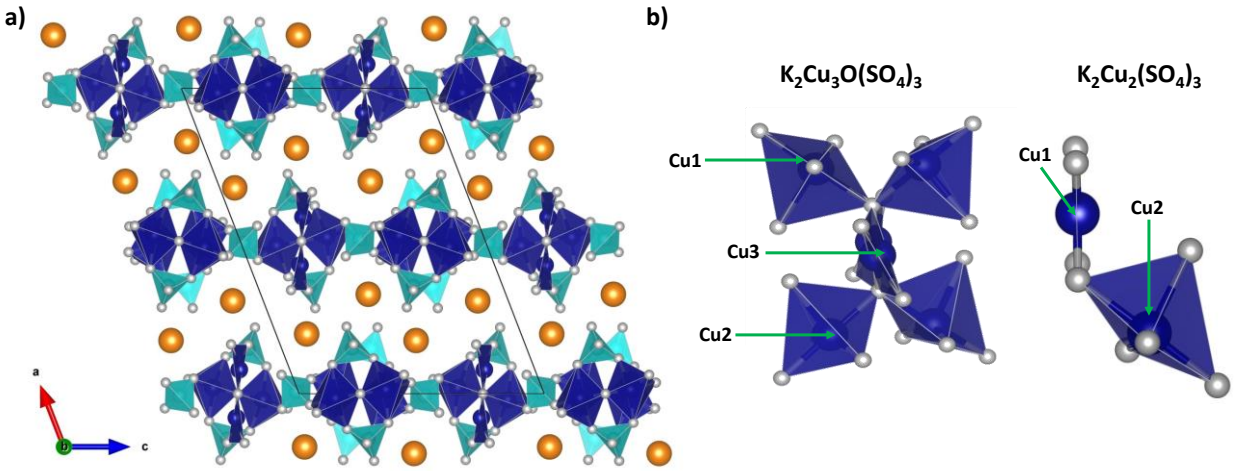

Figure 10: a) Structure of $K_2Cu_3O(SO_4)_3$, which adopts a layered-like structure as shown along the b-axis. The Cu-based polyhedra (CuO_5 and CuO_4) and SO_4 tetrahedra are shown in blue and light blue, respectively. Oxygen and potassium atoms are illustrated as grey and orange spheres. b) Local coordination of Cu-based polyhedra in $K_2Cu_3O(SO_4)_3$ and $K_2Cu_2(SO_4)_3$.

Unfortunately, our trials to remove K^+ from $K_2Cu_3O(SO_4)_3$ (theoretical capacity: 109 mAh/g) failed, regardless of the route (chemical or electrochemical) and conditions we tried. Nevertheless, since both $K_2Cu_2(SO_4)_3$ and $K_2Cu_3O(SO_4)_3$ compounds are part of the family of S = 1/2 systems, which have been intensively studied for magnetic properties, we wanted to check for a possible transition into a magnetically ordered state. We therefore recorded neutron powder diffraction patterns at temperatures ranging from 1.6 K to 290 K (Figure SI6). All NPD patterns are superimposable over the whole temperature range (expect for a small shift of peaks resulting from a cell contraction on cooling) implying the absence of magnetic long range ordering. Moreover, the unchanged background at low temperature suggests the absence also of short range correlations. This does not come as a surprise since the topology of the two compounds reveal rather isolated Cu^{2+} atoms. Further studies on the magnetic behaviors of these compounds are desirable.

Conclusions

In previous reports, new polyanionic host structures for Li^+ and Na^+ insertion have been stabilized through K^+ extraction from their mother phase. We have here reported an extension of this concept to the langbeinite $K_2Fe_2(SO_4)_3$ phase, which shows, however, poor electrochemical activity owing to its structural instabilities upon K^+ extraction. Further exploring the $A_2M_2(SO_4)_3$ family, we synthesized a novel $K_2Cu_2(SO_4)_3$ member via a solid state

approach that crystallizes in an orthorhombic unit cell (space group $P2_12_12_1$) different from the one of the langbeinite phases. $K_2Cu_2(SO_4)_3$, which presents moderate electrochemical properties, is shown to transform upon heating to the naturally occurring mineral fedotovite $K_2Cu_3O(SO_4)_3$, which is prepared for the first time synthetically. In light of these findings, we can conclude that although the approach of stabilizing new host structures from K-based polyanionic materials is highly interesting, it cannot be fully generalized. Lastly, even though $K_2Cu_2(SO_4)_3$ nor $K_2Cu_3O(SO_4)_3$ are suitable as cathode materials, both compounds present a S=1/2 system and therefore might display interesting magnetic properties.

Supporting Information

Details on Bond Valence Energy Landscape (BVEL) calculations and resulting BVELs of $K_2Fe_2(SO_4)_3$ and $K_2Cu_2(SO_4)_3$; low magnification HAADF-STEM image of $K_2Cu_2(SO_4)_3$ particles; Rietveld refinement of chemically oxidized $K_2Cu_2(SO_4)_3$; pictures of $K_2Cu_2(SO_4)_3$ and $K_2Cu_3O(SO_4)_3$ powders; neutron powder patterns of $K_2Cu_2(SO_4)_3$ and $K_2Cu_3O(SO_4)_3$. CIF files of $K_2Fe_2(SO_4)_3$, $K_2Cu_2(SO_4)_3$ and $K_2Cu_3O(SO_4)_3$.

Acknowledgements

We thank Matthieu Courty for performing TGA/DSC measurements. Use of the 11-BM mail service of the APS at Argonne National Laboratory was supported by the U.S. Department of Energy under Contract DE-AC02-06CH11357 and is acknowledged. The French CRG D1B is acknowledged for allocating neutron beamtime. L.L. thanks the ANR “Hipolite” for the PhD funding.

Author Information Notes

* Corresponding author: jean-marie.tarascon@college-de-france.fr

References

(1) Padhi, A. K.; Nanjundaswamy, K. S.; Masquelier, C.; Goodenough, J. B. Mapping of Transition Metal Redox Energies in Phosphates with NASICON Structure by Lithium Intercalation. *J. Electrochem. Soc.* **1997**, *144*, 2581–2586.

(2) Masquelier, C.; Croguennec, L. Polyanionic (Phosphates, Silicates, Sulfates) Frameworks as Electrode Materials for Rechargeable Li (or Na) Batteries. *Chem. Rev.* **2013**, *113*, 6552–6591.

(3) Barpanda, P.; Ati, M.; Melot, B. C.; Rousse, G.; Chotard, J.-N.; Doublet, M.-L.; Sougrati, M. T.; Corr, S. A.; Jumas, J.-C.; Tarascon, J.-M. A 3.90 V Iron-Based Fluorosulphate Material for Lithium-Ion Batteries Crystallizing in the Triplite Structure. *Nat. Mater.* **2011**, *10*, 772–779.

(4) Ati, M.; Sathiya, M.; Boulineau, S.; Reynaud, M.; Abakumov, A.; Rousse, G.; Melot, B.; Van Tendeloo, G.; Tarascon, J.-M. Understanding and Promoting the Rapid Preparation of the *Triplite* -Phase of $LiFeSO_4$ F for Use as a Large-Potential Fe Cathode. *J. Am. Chem. Soc.* **2012**, *134*, 18380–18387.

(5) Ati, M.; Melot, B. C.; Chotard, J.-N.; Rousse, G.; Reynaud, M.; Tarascon, J.-M. Synthesis and Electrochemical Properties of Pure $LiFeSO_4F$ in the Triplite Structure. *Electrochem. Commun.* **2011**, *13*, 1280–1283.

(6) Recham, N.; Rousse, G.; Sougrati, M. T.; Chotard, J.-N.; Frayret, C.; Mariyappan, S.; Melot, B. C.; Jumas, J.-C.; Tarascon, J.-M. Preparation and Characterization of a Stable $FeSO_4F$-Based Framework for Alkali Ion Insertion Electrodes. *Chem. Mater.* **2012**, *24*, 4363–4370.

(7) Ling, C.; Mizuno, F. Mechanistic Study of the Electrochemical Extraction of K^+ from $KFeSO_4F$. *J. Mater. Chem. A* **2013**, *1*, 8000–8006.

(8) Lander, L.; Rousse, G.; Abakumov, A. M.; Sougrati, M.; Tendeloo, G. van; Tarascon, J.-M. Structural, Electrochemical and Magnetic Properties of a Novel $KFeSO_4F$ Polymorph. *J. Mater. Chem. A* **2015**, *3*, 19754–19764.

(9) Fedotov, S. S.; Khasanova, N. R.; Samarin, A. S.; Drozhzhin, O. A.; Batuk, D.; Karakulina, O. M.; Hadermann, J.; Abakumov, A. M.; Antipov, E. V. $AVPO_4F$ (A = Li, K): A 4 V Cathode Material for High-Power Rechargeable Batteries. *Chem. Mater.* **2016**, *28*, 411–415.

(10) Manthiram, A.; Goodenough, J. B. Lithium Insertion into $Fe_2(SO_4)_3$ Frameworks. *J. Power Sources* **1989**, *26*, 403–408.

(11) Wu, Q.; Xu, Y.; Ju, H. New-Type Low-Cost Cathode Materials for Li-Ion Batteries: Mikasaite-Type $Fe_2(SO_4)_3$. *Ionics* **2012**, *19*, 471–475.

(12) Barpanda, P.; Oyama, G.; Nishimura, S.; Chung, S.-C.; Yamada, A. A 3.8-V Earth-Abundant Sodium Battery Electrode. *Nat. Commun.* **2014**, *5*.

(13) Oyama, G.; Pecher, O.; Griffith, K. J.; Nishimura, S.; Pigliapochi, R.; Grey, C. P.; Yamada, A. Sodium Intercalation Mechanism of 3.8 V Class Alluaudite Sodium Iron Sulfate. *Chem. Mater.* **2016,** *28*, 21-5328.

(14) Zemann, A.; Zemann, J. Die Kristallstruktur von Langbeinit, K2Mg2(SO4)3. *Acta Crystallogr. 10*, 409–413.

(15) Oelkrug, H.; Brückel, T.; Hohlwein, D.; Hoser, A.; Prandl, W. The Magnetic Structure of the Langbeinite $K_2Mn_2(SO_4)_3$. *Phys. Chem. Miner.* **1988**, *16*, 246–249.

(16) Emmenegger, F. Crystal Growth and Electro-Optic Effect of Some Double Sulfates with the Langbeinite Structure. *J. Appl. Phys.* **1968**, *39*, 3039.

(17) Hernández-Rodríguez, C.; Geday, M. A.; Kreisel, J.; Glazer, A. M.; Hidalgo-López, A. Optical Birefringence Imaging of the Phase Transition of $K_2Mn_2(SO_4)_3$. *J. Appl. Crystallogr.* **2003**, *36*, 914–919.

(18) Speer, D.; Salje, E. Phase Transitions in Langbeinites I: Crystal Chemistry and Structures of K-Double Sulfates of the Langbeinite Type $M_2^{2+}K_2(SO_4)_3$, M^{2+}= Mg, Ni, Co, Zn, Ca. *Phys. Chem. Miner.* **1986**, *13*, 17–24.

(19) Windhaus, M.; Mosel, B. D.; Muller-Warmuth, W. Moessbauer Studies of Fe^{2+} in Iron Langbeinites and Other Crystals with Langbeinite Structure. *Z. Naturforschung -J. Phys. Sci.* **1998**, *53*, 27–37.

(20) Abrahams, S. C.; Bernstein, J. L. Piezoelectric Langbeinite-Type $K_2Cd_2(SO_4)_3$: Room Temperature Crystal Structure and Ferroelastic Transformation. *J. Chem. Phys.* **1977**, *67*, 2146.
(21) Abrahams, S. C.; Lissalde, F.; Bernstein, J. L. Piezoelectric Langbeinite-Type $K_2Cd_2(SO_4)_3$ Structure at Four Temperatures below and One above the 432°K Ferroelastic–paraelastic Transition. *J. Chem. Phys.* **1978**, *68*, 1926.
(22) Rietveld, H. M. A Profile Refinement Method for Nuclear and Magnetic Structures. *J. Appl. Crystallogr.* **1969**, *2*, 65–71.
(23) Rodríguez-Carvajal, J. *FullProf Suite*; www.ill.eu/sites/fullprof/; www.ill.eu/sites/fullprof/.
(24) Rodriguez-Carvajal, J. Recent Advances in Magnetic Structure Determination by Neutron Powder Diffraction. *Phys. B Condens. Matter* **1993**, *192*, 55.
(25) Boultif, A. History of the Dichotomy Method for Powder Pattern Indexing. *Powder Diffr.* **2005**, *20*, 284–287.
(26) Boultif, A.; Louër, D. Indexing of Powder Diffraction Patterns for Low-Symmetry Lattices by the Successive Dichotomy Method. *J. Appl. Crystallogr.* **1991**, *24*, 987–993.
(27) FoxWiki - FOX, Free Objects for Crystallography Wiki http://fox.vincefn.net/.
(28) Favre-Nicolin, V.; Cerny, R. FOX, `free Objects for Crystallography': a Modular Approach to Ab Initio Structure Determination from Powder Diffraction. *J. Appl. Crystallogr.* **2002**, *35*, 734–743.
(29) Gattow, G.; Zemann, J. Über Doppelsulfate Vom Langbeinit-Typ A<sup>2+</sub>$B^{2+}(SO_4)_3$. *Z Anorg Allg Chem* **1958**, *293*, 233–240.
(30) Bronw, I. D.; Altermatt, D. Bond-Valence Parameters Obtained from a Systematic Analysis of the Inorganic Crystal Structure Database. *Acta Crystallogr.* **1985**, *B41*, 244–247.
(31) Adams, S. From Bond Valence Maps to Energy Landscapes for Mobile Ions in Ion-Conducting Solids. *Solid State Ion.* **2006**, *177*, 1625–1630.
(32) Sun, M.; Rousse, G.; Abakumov, A. M.; Saubanère, M.; Doublet, M.-L.; Rodríguez-Carvajal, J.; Van Tendeloo, G.; Tarascon, J.-M. $Li_2Cu_2O(SO_4)_2$: A Possible Electrode for Sustainable Li-Based Batteries Showing a 4.7 V Redox Activity vs Li^+/Li^0. *Chem. Mater.* **2015**, *27*, 3077–3087.
(33) Lander, L.; Reynaud, M.; Carrasco, J.; Katcho, N. A.; Bellin, C.; Polian, A.; Baptiste, B.; Rousse, G.; Tarascon, J.-M. Unveiling the Electrochemical Mechanisms of the $Li_2Fe(SO_4)_2$ Polymorphs by Neutron Diffraction and Density Functional Theory Calculations. *Phys. Chem. Chem. Phys.* **2016**, *18*, 14509–14519.
(34) Rangan, K. K.; Gopalakrishnan, J. New Titanium-Vanadium Phosphates of Nasicon and Langbeinite Structures, and Differences between the Two Structures toward Deintercalation of Alkali Metal. *J. Solid State Chem.* **1994**, *109*, 116–121.
(35) Delacourt, C.; Laffont, L.; Bouchet, R.; Wurm, C.; Leriche, J.-B.; Morcrette, M.; Tarascon, J.-M.; Masquelier, C. Toward Understanding of Electrical Limitations (Electronic, Ionic) in LiMPO[sub 4] (M=Fe, Mn) Electrode Materials. *J. Electrochem. Soc.* **2005**, *152*, A913.
(36) Sun, M.; Rousse, G.; Corte, D. D.; Saubanère, M.; Doublet, M.-L.; Tarascon, J.-M. A Fully Ordered Triplite, $LiCuSO_4F$. *Chem. Mater.* **2016**, *28*, 1607–1610.
(37) Starova, G. L.; Filatov, S. K.; Fundamensky, V. S.; Vergasova, L. P. The Crystal Structure of Fedotovite, $K_2Cu_3O(SO_4)_3$. *Mineral. Mag.* **1991**, *55*, 613–616.

Tables

Table 1: Crystallographic data and atomic positions of $K_2Fe_2(SO_4)_3$ deduced from Rietveld refinements of its X-ray powder diffraction pattern. The isotropic temperature values (B_{iso}) and the results from Bond Valence Sum (BVS) analyses are listed in last two columns.

Cubic $K_2Fe_2(SO_4)_3$

Space group $P2_13$			R_{Bragg} = 3.42 %		χ^2 = 1.50		
a = 10.00478(3) Å			V = 1001.433(6) Å^3				
Atom	Wyckoff position	x	y	z	Occupancy	B_{iso} (Å^2)	BVS
K1	4*a*	0.8135(3)	0.8135(3)	0.8135(3)	1	2.21(7)	1.14(1)
K2	4*a*	0.0502(3)	0.0502(3)	0.0502(3)	1	2.21(7)	1.00(1)
Fe1	4*a*	0.3350(2)	0.3350(2)	0.3350(2)	1	1.39(4)	2.19(2)
Fe2	4*a*	0.59432(17)	0.59432(17)	0.59432(17)	1	1.39(4)	1.93(2)
S1	12*b*	0.2210(3)	0.3760(5)	0.0174(4)	1	1.41(6)	6.41(8)
O1	12*b*	0.3108(8)	0.2798(8)	0.9597(7)	1	2.59(9)	2.18(4)
O2	12*b*	0.0845(8)	0.3244(9)	0.0066(7)	1	2.59(9)	2.06(4)
O3	12*b*	0.2353(7)	0.4970(10)	0.9388(11)	1	2.59(9)	2.14(5)
O4	12*b*	0.2540(6)	0.4088(7)	0.1541(9)	1	2.59(9)	2.12(4)

Table 2: Crystallographic data and atomic positions of $K_2Cu_2(SO_4)_3$ determined from Rietveld refinements of its synchrotron X-ray powder diffraction pattern. The isotropic temperature values (B_{iso}) and the results from Bond Valence Sum (BVS) analyses are listed in last two columns.

Orthorhombic $K_2Cu_2(SO_4)_3$

Space group $P2_12_12_1$			R_{Bragg} = 4.84 %			χ^2 = 1.05	
a = 4.81065(1)Å		*b* = 11.91795(3) Å	*c* = 18.67516(4) Å			*V* = 1070.704(4) Å^3	
Atom	Wyckoff position	*x*	*y*	*z*	Occupancy	B_{iso} (Å^2)	BVS
K1	4*a*	0.18250(32)	0.13076(11)	0.40811(7)	1	1.914(39)	1.05(1)
K2	4*a*	0.69591(38)	0.32848(11)	0.18436(7)	1	1.519(40)	1.30(1)
Cu1	4*a*	0.24424(32)	0.48396(5)	0.34274(4)	1	1.330(17)	1.87(1)
Cu2	4*a*	0.24010(22)	0.11442(7)	0.05180(3)	1	1.085(15)	1.94(1)
S1	4*a*	0.24667(54)	0.11663(12)	0.21865(7)	1	0.797(28)	5.82(3)
O1	4*a*	0.16573(91)	0.03348(30)	0.27297(21)	1	1.520(108)	1.93(2)
O2	4*a*	0.07946(73)	0.08287(30)	0.15149(23)	1	0.498(95)	2.08(2)
O3	4*a*	0.20298(113)	0.23147(33)	0.23780(17)	1	1.765(103)	1.98(2)
O4	4*a*	0.54695(74)	0.11448(35)	0.19594(19)	1	0.592(95)	2.05(2)
S2	4*a*	0.20980(42)	0.38040(14)	0.04783(8)	1	1.027(32)	5.96(3)
O5	4*a*	0.19490(104)	0.60269(34)	0.47395(17)	1	1.552(102)	1.80(2)
O6	4*a*	0.31752(84)	0.27285(33)	0.07609(16)	1	0.582(92)	2.08(2)
O7	4*a*	0.89854(76)	0.37610(36)	0.04664(21)	1	1.073(106)	2.05(2)
O8	4*a*	0.29464(111)	0.46651(27)	0.09906(19)	1	1.109(96)	1.80(2)
S3	4*a*	0.23111(46)	0.14077(12)	0.59875(8)	1	0.864(32)	5.94(3)
O9	4*a*	0.06258(72)	0.11974(37)	0.66422(19)	1	0.544(89)	2.00(2)
O10	4*a*	0.18384(109)	0.05074(29)	0.54712(20)	1	1.538(119)	2.15(2)
O11	4*a*	0.16777(78)	0.24878(39)	0.56824(17)	1	0.844(92)	1.99(2)
O12	4*a*	0.03586(73)	0.35793(32)	0.37840(20)	1	0.509(90)	1.96(2)

Table 3: Crystallographic data and atomic positions of $K_2Cu_3O(SO_4)_3$ determined from the Rietveld refinement of its synchrotron XRD pattern. The isotropic temperature values (B_{iso}) were constrained identical for a same chemical species. Results from Bond Valence Sum (BVS) analyses are listed in last column.

Monoclinic fedotovite $K_2Cu_3O(SO_4)_3$

*Space group C*2/*c*		R_{Bragg} = 2.45 %					χ^2 = 6.17
a = 19.09059(5) Å		*b* = 9.52853(2) Å		*c* = 14.18650(3) Å	β = 110.63109(19)°		*V* = 2415.100(9) Å^3
Atom	Wyckoff position	*x*	*y*	*z*	Occupancy	B_{iso} (Å^2)	BVS
K1	8*f*	0.32450(11)	0.7499(3)	0.43781(15)	1	2.56(4)	1.42(2)
K2	8*f*	0.19534(12)	0.7348(3)	0.12292(15)	1	2.56(4)	0.85(2)
Cu1	8*f*	0.48124(6)	0.01768(14)	0.34270(8)	1	0.681(13)	2.06(2)
Cu2	8*f*	0.48655(6)	0.47906(14)	0.14051(8)	1	0.681(13)	2.16(2)
Cu3	8*f*	0.42128(6)	0.74630(16)	0.20640(8)	1	0.681(13)	1.99(2)
S1	8*f*	0.50556(13)	0.7495(3)	0.49027(17)	1	0.70(3)	5.92(1)
S2	8*f*	0.64718(12)	0.0260(3)	0.36632(18)	1	0.70(3)	6.02(1)
S3	8*f*	0.35189(13)	0.4676(3)	0.21723(17)	1	0.70(3)	5.90(1)
O1	4*e*	0.5	0.8869(9)	0.25	1	0.81(4)	1.98(16)
O2	8*f*	0.4511(3)	0.8272(5)	0.4080(4)	1	0.81(4)	2.01(2)
O3	8*f*	0.5611(3)	0.6769(5)	0.4581(4)	1	0.81(4)	1.91(3)
O4	8*f*	0.4635(3)	0.6458(5)	0.5274(4)	1	0.81(4)	2.21(3)
O5	8*f*	0.5892(3)	0.0595(6)	0.4100(4)	1	0.81(4)	2.05(3)
O6	8*f*	0.4042(3)	0.4419(5)	0.3152(4)	1	0.81(4)	2.26(3)
O7	8*f*	0.3389(3)	0.6224(6)	0.2028(4)	1	0.81(4)	2.06(3)
O8	8*f*	0.2808(3)	0.3954(5)	0.2008(4)	1	0.81(4)	1.93(3)
O9	8*f*	0.5479(3)	0.8486(5)	0.5736(4)	1	0.81(4)	2.03(2)
O10	8*f*	0.6200(3)	0.0691(5)	0.2584(4)	1	0.81(4)	1.89(2)
O11	8*f*	0.3894(3)	0.4208(5)	0.1415(4)	1	0.81(4)	1.77(3)
O12	4*e*	0.5	0.6045(9)	0.25	1	0.81(4)	2.04(16)
O13	8*f*	0.6611(3)	0.8718(6)	0.3713(4)	1	0.81(4)	1.98(3)
O14	8*f*	0.7160(3)	0.0942(5)	0.4226(4)	1	0.81(4)	2.23(3)

For Table of Contents Only

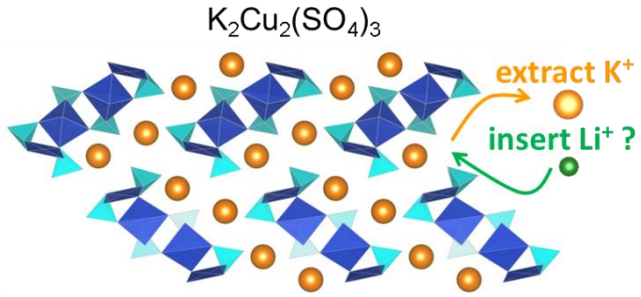

The possibility of extracting K to re-insert Li from langbeinite $K_2Fe_2(SO_4)_3$ is evaluated. A new copper-based compound $K_2Cu_2(SO_4)_3$ is reported for the first time and its structure determined. The electrochemical behavior of $K_2Cu_2(SO_4)_3$ against Li is explored, and its relation to fedotovite $K_2Cu_3O(SO_4)_3$ revealed.